

## Collisions of Small Kuiper Belt Objects With (486958) Arrokoth: Implications for Its Spin Evolution and Bulk Density

### Key Points:

- Impacts of classical Kuiper belt objects consistent with Arrokoth's observed craters caused at best modest spin changes
- The formation of the largest craters would have had a larger effect, especially if cratering efficiency is reduced by substantial porosity
- The most consistent interpretation of Arrokoth's shape and slow spin is that its bulk density is low, between 250 and 400 kg m<sup>-3</sup>

### Supporting Information:

Supporting Information may be found in the online version of this article.




### Correspondence to:

X. Mao,  
[xiaochen.mao@wustl.edu](mailto:xiaochen.mao@wustl.edu)

### Citation:

Mao, X., McKinnon, W. B., Singer, K. N., Keane, J. T., Beyer, R. A., Greenstreet, S., et al. (2021). Collisions of small Kuiper belt objects with (486958) Arrokoth: Implications for its spin evolution and bulk density. *Journal of Geophysical Research: Planets*, 126, e2021JE006961. <https://doi.org/10.1029/2021JE006961>

Received 24 MAY 2021  
Accepted 22 NOV 2021

Xiaochen Mao<sup>1</sup> , William B. McKinnon<sup>1</sup> , Kelsi N. Singer<sup>2</sup> , James T. Keane<sup>3</sup> , Ross A. Beyer<sup>4,5</sup> , Sarah Greenstreet<sup>6,7</sup> , Stuart J. Robbins<sup>2</sup> , Paul M. Schenk<sup>8</sup> , Jeffrey M. Moore<sup>5</sup> , S. Alan Stern<sup>2</sup> , Harold A. Weaver<sup>9</sup> , John R. Spencer<sup>2</sup> , Catherine B. Olkin<sup>2</sup> , and the New Horizons Science Team

<sup>1</sup>Department of Earth and Planetary Sciences and McDonnell Center for the Space Sciences, Washington University in St. Louis, St. Louis, MO, USA, <sup>2</sup>Southwest Research Institute, Boulder, CO, USA, <sup>3</sup>Jet Propulsion Laboratory, California Institute of Technology, Pasadena, CA, USA, <sup>4</sup>SETI Institute, Mountain View, CA, USA, <sup>5</sup>NASA Ames Research Center, Moffett Field, CA, USA, <sup>6</sup>Asteroid Institute, Mill Valley, CA, USA, <sup>7</sup>Department of Astronomy and the DIRAC Institute, University of Washington, Seattle, WA, USA, <sup>8</sup>LPI, Houston, TX, USA, <sup>9</sup>JHUAPL, Laurel, MD, USA

**Abstract** The orientation and morphology of the bilobate, cold classical Kuiper belt object (486958) Arrokoth (formerly 2014 MU<sub>69</sub>) is consistent with a slow, tidal merger of a close binary. However, the discrepancy between Arrokoth's present-day rotation (15.9 hr) and synchronous rotation for nominal cometary densities near ~500 kg/m<sup>3</sup> implies reduction (up to 30%) in post-merger spin angular momentum. We investigate how collisions with dynamically cold and hot classical Kuiper belt objects might have affected Arrokoth's post-merger spin. Using a dynamically equivalent triaxial ellipsoid, 5000 Monte Carlo simulations of 100 impacts each, consistent with Arrokoth's cratering record, were carried out. Starting from the assumption of critical, synchronous rotation for a given density, these simulations rarely reproduce Arrokoth's present spin period, unless its true density is near 250 kg/m<sup>3</sup>. We explore in greater depth the effects of formation of Arrokoth's largest crater (now officially named Sky, previously informally named Maryland). We adopt point-source scaling and randomly select impact parameters that lead to the crater, using Arrokoth's full bilobate shape. Results from Sky's formation alone are similar to those considering a full range of impactor sizes, unless we adopt low cratering efficiency due to high porosity, which implies substantially larger Sky-forming impactors. Overall, results imply that the probability of substantial angular momentum change due to impacts alone over Solar System history is unlikely, and spindown from a synchronous, tidal rotation rate to a 15.9-hr period unlikely unless Arrokoth itself was and is a very low density object (~250 kg/m<sup>3</sup>), though we cannot statistically rule out densities up to 400 kg/m<sup>3</sup>.

**Plain Language Summary** Both lobes of the cold classical Kuiper belt object Arrokoth were likely in a close spin-synchronous orbit before they gently merged to form the bilobate body we see today. This spin-synchronous orbital period depends on density, however, and Arrokoth's observed spin period implies that it either has an extremely low density (much lower than typical cometary values) or underwent significant despinning after the merger. Here we study the spin-altering effects of impacts by other, small Kuiper belt objects over time and address the likelihood of the required despinning by impacts, with implications for Arrokoth's bulk density. We use a Monte Carlo impact simulation to investigate Arrokoth's rotational response over its impact history, with special attention to the largest recognized crater (Sky). Our results indicate that: (a) Small impacts alone are not capable of altering Arrokoth's spin by much; (b) The likelihood of geophysically significant impact despinning on Arrokoth is low, if it has a typical cometary density of ~500 kg m<sup>-3</sup>; (c) Arrokoth's bulk density may actually be quite low, ~250 kg m<sup>-3</sup>, implying substantial porosity.

### 1. Introduction

The *New Horizons* flyby of (486958) Arrokoth (formerly 2014 MU<sub>69</sub>) on 1 January 2019 revealed a contact binary planetesimal, likely the most primitive object yet visited by spacecraft (Stern et al., 2019). From Arrokoth's detailed shape, the principal axes of each individual lobe were found to be aligned to within a few degrees (Spencer et al., 2020), a configuration that suggests a co-orbiting Arrokoth before a tidally aligned, gentle ( $\lesssim$  few m s<sup>-1</sup>)

merger of its two lobes (McKinnon et al., 2020; Stern et al., 2019). In addition, a large fraction of cold classical Kuiper belt objects (CCKBOs) are telescopic binaries, and the leading hypothesis for their formation is gravitational collapse of overdense particle/pebble swarms in the solar nebula (Nesvorný et al., 2010, 2019, 2021); for plausible swarm angular momentum densities, binaries (or triples, etc.) efficiently form. After these primordial co-orbiting binaries form and if they can shed angular momentum, then in principle their mutual orbit evolution can lead to final mergers, forming contact bilobate bodies like Arrokoth (Grishin et al., 2020; Lyra et al., 2021; McKinnon et al., 2019, 2020).

For Arrokoth, its presumed gentle merger may have occurred at a critical rotation period of 11.26 hr. This value is derived from the mutual gravitational attraction between two barely touching lobes, assuming a comet 67P/Churyumov-Gerasimenko-like bulk density of  $500 \text{ kg m}^{-3}$  (cf. McKinnon et al., 2020; Spencer et al., 2020). If so, Arrokoth's present-day rotation of  $15.92 \pm 0.02 \text{ hr}$  (Stern et al., 2019) would indicate despinning. (We note that analysis over a longer timebase, i.e., one including pre-encounter stellar occultations, gives a refined rotation rate for Arrokoth of  $15.9380 \pm 0.0005 \text{ hr}$  (Buie et al., 2020), a trivial difference of no consequence to this work.) Arrokoth's actual bulk density remains unknown, as does the amount of spin angular momentum Arrokoth may have lost or gained during its evolution. Many mechanisms may potentially influence a small body's spin including tides, collisions, 3-body interactions, YORP and BYORP, Kozai-Lidov oscillations, and gas drag (see McKinnon et al., 2020 and Lyra et al., 2021). Here we explore in detail whether collisions with other KBOs could have substantially altered Arrokoth's spin state throughout geologic time and assess the possibilities of a spindown scenario to explain its observed rotation.

To investigate this problem, we adapt our existing Monte Carlo impact simulations for Ceres and Vesta (Mao & McKinnon, 2020) to fit Arrokoth's impact environment. We first introduce the changes from our previous modeling, such as a triaxial ellipsoid representation and the impactor size-frequency and velocity distributions (Section 2). Then we present different simulation results, based on various combinations of model parameters and assumptions (Section 3). We explicitly investigate the dynamical effects from the singular Sky-forming event in Section 4, adopting a full bilobate model of Arrokoth. A summary and conclusion follows (Section 5).

## 2. Methods and Model Assumptions

The Monte Carlo impact model for asteroids is documented in our previous work (Mao & McKinnon, 2020). However, to simulate Arrokoth's spin evolution, adaptations and modifications need to be made. Thus, in this section, we discuss the following aspects: (a) Geometry of Arrokoth in the model; (b) Impactor size range and total number in Arrokoth's Kuiper belt environment; (c) Impact velocity distribution; and (d) Initial spin and density of Arrokoth.

### 2.1. Arrokoth as a Triaxial Ellipsoid

The shape model derived from stereo-images and global shape (Spencer et al., 2020) clearly shows the bilobate configuration of Arrokoth (Figure 1)—a Large Lobe and a Small Lobe connected at a “neck” (Stern et al., 2021). In earlier work, we presented Arrokoth's spin change due to collisions by modeling Arrokoth as two co-rotating oblate spheroids (Mao et al., 2020b). However, such a geometry inevitably introduces complexities in the impactor and ejecta trajectories, particularly for impacts near the neck region (i.e., where both lobes face each other). While such a modeled shape representation guarantees good correspondence with Arrokoth's actual physical properties, we judged it to be unnecessarily geometrically complex for the questions we were posing. For this reason, we took an alternative approach to represent Arrokoth's shape in the simulation—a triaxial ellipsoid. Spencer et al. (2020) found the best-fit ellipsoidal shape for Arrokoth is (36, 20, 10) km, but this has  $\sim 20\%$  more volume than Arrokoth. Here we argue that, for impact simulation verisimilitude, the cross-sectional area of a target body is a more important factor to match. Thus, below we derive a nearly dynamically equivalent triaxial shape for Arrokoth (with semi major axes  $a > b > c$ ), aiming to match Arrokoth's cross-sectional areas along all three principal axes of figure and its principal moments-of-inertia.

For almost all Arrokoth impactors, gravitational focusing is minimal, given that the escape velocity of a spherically equivalent Arrokoth is only about a few  $\text{m s}^{-1}$ , compared with the typical collisional speed with Arrokoth

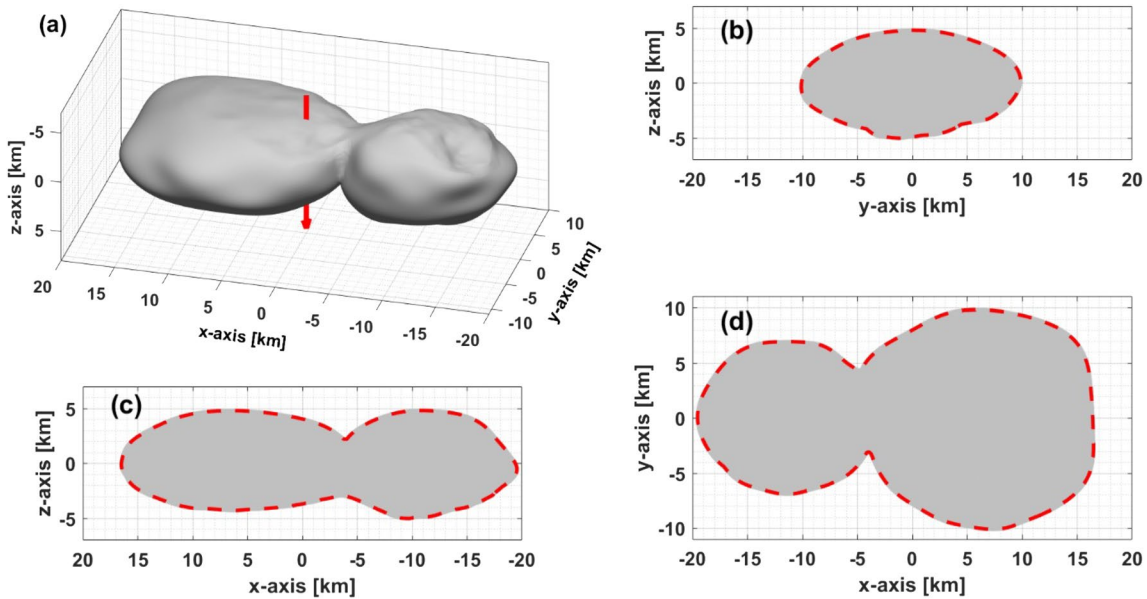


**Figure 1.** Arrokoth shape model and projections along all principal axes of figure. (a) Shape model from Spencer et al. (2020); arrow is spin axis. (b–d) Cross-sections along the  $+x$ ,  $+y$ , and  $+z$  directions, respectively. Dashed curves indicate the boundary of Arrokoth's projection on the  $xy$ -,  $xz$ -, and  $yz$ -planes.

of several hundred  $\text{m s}^{-1}$  (Greenstreet et al., 2019). Thus, the collisional cross-section area, along each principal axis direction, for a given impactor is simply the projection of Arrokoth on three principal planes. Using the shape model (Spencer et al., 2020), we calculate the enclosed area along each of the principal axes (see Figure 1), aligning these directions with the  $+x$ ,  $+y$ , and  $+z$  axes (body-centered) of our modeled triaxial Arrokoth. We fix the longest dimension of this ellipsoid ( $\equiv 2a$ ) to match the real Arrokoth at 36 km and determine the lengths of the  $b$ - and  $c$ -axes from the projections along the  $z$  and  $y$  axes, respectively, yielding  $b = 9.1$  km and  $c = 4.8$  km. The projected area along the  $x$  axis is  $137 \text{ km}^2$  (Figure 1b), 93% of the  $147 \text{ km}^2$  projected area from the shape model (Figure 1d), and this triaxial ellipsoid has a volume only 3% larger than the true Arrokoth, well within the uncertainty of the shape model (see Table 1 for all parameters). Hereafter, we refer to this model triaxial ellipsoid as triaxial-Arrokoth, or TA (see Supporting Information S1).

**Table 1**

Parameters Used in the Initial Simulations for Triaxial-Arrokoth

Arrokoth density ( $\rho$ ) <sup>a</sup>	$500 \text{ kg m}^{-3}$
Triaxial-Arrokoth (TA) density <sup>a</sup>	$619 \text{ kg m}^{-3}$
TA dimensions ( $a, b, c$ ) <sup>b</sup>	(18.0, 9.1, 4.8) km
TA mass ( $M$ )	$2.03 \times 10^{15} \text{ kg}$
Initial spin period ( $P_0$ ) <sup>c</sup>	11.26 hr
Number of impacts <sup>d</sup>	100
Impactor diameter range ( $d$ ) <sup>e</sup>	[10 m, 1 km]
Impactor velocity range ( $U$ ) <sup>e</sup>	$[V_{\text{esc}}, 5.3 \text{ km s}^{-1}]$

<sup>a</sup>Scaled to match Arrokoth's principal moment-of-inertia from its shape model (Keane et al., 2020). <sup>b</sup>Largely preserves Arrokoth's cross-sectional areas along each principal axis. <sup>c</sup>Synchronous rotation corresponding to true  $\rho = 500 \text{ kg m}^{-3}$ . Varies with assumed  $\rho$  (Equation 2). <sup>d</sup>40–50 craters or pits  $\geq 0.2$  km wide were identified in *New Horizons* images (Spencer et al., 2020). If the other side of Arrokoth is similar, we expect the total number of craters of these sizes to be of order 100. <sup>e</sup>From the impact velocity probability calculations (Figure 2 in Greenstreet et al., (2019)). The upper bound is for hot classical KBOs. The lower bound is the escape velocity at the impact location (see Figure 4), about  $4\text{--}5 \text{ m s}^{-1}$  in general.

## 2.2. Impactor Velocity

Due to their immense heliocentric distance, impacts among KBOs occur at generally much lower speeds than, say, among the asteroids. Greenstreet et al. (2019) calculated the impact rates on Arrokoth by considering collisions from all possible KBO subpopulations (see their Table 1). Each subpopulation contributes differently to the overall cratering history on Arrokoth, with varying impact velocity distributions. For Arrokoth, four KBO subpopulations are particularly important impactor sources: cold classicals, hot classicals, outer classicals, and the 3:2 Neptune-resonant population (the plutinos). In terms of their impact velocity characteristics, these four subgroups can be divided into two categories based on velocity: the majority of impacts (76%) are due to the cold classicals, whose low orbital eccentricities and inclinations guarantee relatively slow collisions, while hot classicals represent the high velocity subpopulations (i.e., hot, outer, and 3:2 resonant subpopulations) reasonably well (cf. Abedin et al., 2021). We thus assume the remaining 24% are represented by the hot classical KBO velocity distribution. Figure 2 shows the normalized velocity distributions from these two KBO subgroups.

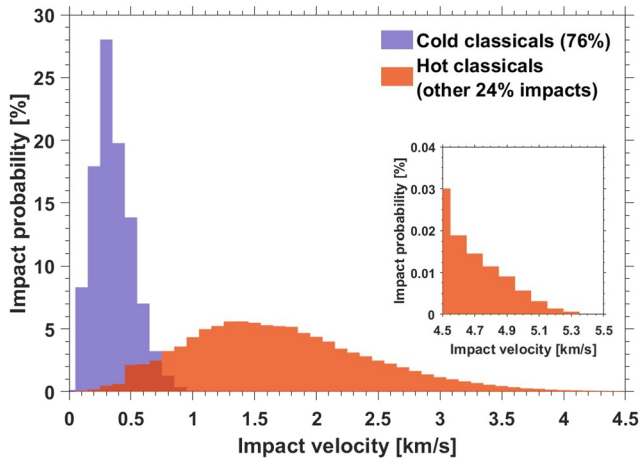


**Figure 2.** Normalized impact velocity distributions at Arrokoth for different KBO subpopulations (from Greenstreet et al., 2019). For cold classicals ( $\approx 76\%$  of the impact flux), impact velocities do not exceed  $1.2 \text{ km s}^{-1}$ , while the most likely impact velocity is  $300 \text{ m s}^{-1}$ . For hot classicals (representative of the rest, see Section 2.2), the most probable impact velocity is  $1.4 \text{ km s}^{-1}$ . The cumulative probability for hot classicals with velocity  $>4 \text{ km s}^{-1}$  is less than  $0.4\%$  (inset, note change in vertical scale).

### 2.3. Total Impactor Number and Size Range

Before *New Horizons*' arrival at Arrokoth, Singer, McKinnon et al. (2019) measured craters on Charon's plains and inferred that the impacting KBO population follows a shallow size-frequency distribution (SFD) close to  $dN \propto d^{-1.75}$  for  $d \lesssim 2 \text{ km}$  (where  $d$  is the KBO diameter and  $dN$  is the differential number of objects), and a steeper SFD for larger KBOs. Images returned by *New Horizons* allowed for the identification of craters and generic "pits" on Arrokoth's surface and 43 features that could potentially be impact craters were identified with varying degrees of confidence (Singer, McKinnon et al., 2019; Spencer et al., 2020), with the smallest about  $0.19 \text{ km}$  wide. Analysis of these potential craters determined a slightly steeper log SFD slope of  $-2.3 \pm 0.6$  for craters smaller than  $10 \text{ km}$  in diameter (Spencer et al., 2020), but we retain  $-1.75$  for the average KBO SFD slope because it is within the uncertainties of the Arrokoth SFD slope and crater identification is more secure on Charon (the relevant slope uncertainties for Charon are  $\sim \pm 0.3$ ; see Table S2 in Singer, McKinnon et al., 2019). The encounter geometry allowed only half of Arrokoth to be seen, thus it is justifiable to assume a similar number of crater-like features on the other side. Although the lighting geometry on the encounter side strongly favors crater detection near the terminator, which may lead to global undercounting, inclusion of those features that could be craters but with low confidence (Spencer et al., 2020) perhaps compensates. We thus approximate the total number of possible impactors in a given simulation to be 100. We constrain the size range of these 100 impactors from crater scaling as follows.

The highest resolution images of Arrokoth identify craters from  $\sim 0.2\text{-km}$  to  $7.2\text{-km}$  wide (see Figure 6 and data S3 in Spencer et al., 2020). Following the impactor-crater scaling in Greenstreet et al. (2019) (which is derived from Holsapple (1993) and Housen and Holsapple (2011) assuming unconsolidated, porous, sand- or regolith-like material properties), we constrain the corresponding impactor size range to be between  $10 \text{ m}$  and  $1 \text{ km}$  to account for the range of crater sizes seen on Arrokoth.

In Greenstreet et al. (2019), the crater-impactor scaling is given as:

$$D = 8.9 \left( \frac{U^2}{g} \right)^{0.170} \left( \frac{\delta}{\rho} \right)^{0.333} d^{0.830} \text{ km}, \quad (1)$$

where  $D$  is the crater diameter (in km),  $U$  is taken to be the vertical component of the impact velocity (in  $\text{km s}^{-1}$ ),  $g$  is the gravitational acceleration (in  $\text{cm s}^{-2}$ ) and  $\delta$  and  $\rho$  are the densities of the impactor and the target respectively (for simplicity, we assume  $\delta = \rho$  throughout this work). The density of Arrokoth was not determined by *New Horizons*, but for a spherically equivalent Arrokoth, its surface gravity  $g = 0.13 \times (\rho/500) \text{ cm s}^{-2}$ . Figure S1 in Supporting Information S1 shows the relation between  $D$  and  $(U, d)$  assuming  $\rho = \delta = 500 \text{ kg m}^{-3}$ . *New Horizons* only identified one multi-km-scale crater—the previously informally named Maryland, now officially named Sky (about  $7\text{-km}$  wide) – and all the others are less than  $1 \text{ km}$  in width. Therefore, we expect most impactors in the simulation to be smaller than  $\sim 100 \text{ m}$  in diameter for a typical cold classical impactor (dashed green line in Figure S1 in Supporting Information S1, at the most likely impact speed), whereas for a typical impactor from the hot classicals (dashed red line in Figure S1 in Supporting Information S1) corresponding sizes are smaller. We set the upper limit impactor size at  $1 \text{ km}$ , to allow for the formation of "Sky-class" craters in the simulation. This upper bound, however, is not fixed; indeed, we will come back to relax its value in Section 3.4, as well as discuss the effects of alternative SFD slopes.

### 2.4. Density and Initial Spin of Arrokoth

Arrokoth's bulk density was not directly determined by *New Horizons* (Stern et al., 2019), but geophysical analyses to date (neck stresses and the gravitational slope distribution in McKinnon et al., 2020 and overall shape stability in Hirabayashi et al., 2020) have yielded a possible density range for Arrokoth, from close to  $250$  to  $\sim 500 \text{ kg m}^{-3}$ . The lower bound, from the neck tensile strength/rotational fission limit, is fairly firm. The upper

bound is plausible, as comet 67P/Churyumov-Gerasimenko's density is very accurately known at  $532 \pm 7 \text{ kg m}^{-3}$ , from *Rosetta* radio-tracking and a highly accurate volume estimate (see Groussin et al., 2019). Preferred density estimates for other Jupiter family comets from non-gravitational force (NGF) modeling are consistent with or lower than the 67P value. For example, comet 9P/Tempel 1 has a preferred density range from 200 to 470  $\text{kg m}^{-3}$ , from NGF and *Deep Impact* ejecta plume modeling; 19P/Borrelly has a preferred density of 490  $\text{kg m}^{-3}$ ; and for 81P/Wild 2 this value is 300  $\text{kg m}^{-3}$  (see Table 1 in Groussin et al., 2019). We note that Jupiter-family comets such as 67P are sourced from the so-called scattered disk of the Kuiper belt, and a close but not exact compositional correspondence is expected between scattered disk objects and cold classical KBOs (Morbidelli & Nesvorný, 2020).

There is, however, a possible deeper link between Arrokoth's bulk density and the synchronous spin of both lobes. Lack of resolvable deformation around Arrokoth's neck implies formation in a gentle merger of the two lobes (McKinnon et al., 2020; Stern et al., 2019), and furthermore may imply critical or synchronous rotation of Arrokoth at the time of the merger (i.e., low stresses across the contact). If so, Arrokoth's observed rotational period of 15.92 hr (Stern et al., 2019) would imply a rather low bulk density, 250  $\text{kg m}^{-3}$ ; following the relation for Arrokoth's critical, synchronous rotational period from McKinnon et al. (2020):

$$P = 15.92 \times (250 \text{ kg m}^{-3} / \rho)^{0.5} \text{ hr} \quad (2)$$

Cometary densities have been variously estimated to lie between 100 and  $\sim 1,000 \text{ kg m}^{-3}$ , with varying degrees of uncertainty (Table 1 in Groussin et al., 2019), so Arrokoth's present spin could imply a change in rotation rate from that at lobe merger, depending on its actual density. Specifically, if Arrokoth's bulk density is more in line with that of 67P, the best-determined cometary value (e.g.,  $\sim 500 \text{ kg m}^{-3}$ ), its critical rotation period would have been much shorter, about 11.3 hr; in this circumstance nearly 30% of its initial angular momentum would have to have been lost or transferred via dynamical or other processes. In this regard, Arrokoth could be considered a rather slow rotator for a contact binary with comet-like density. On the other hand, one may argue that Arrokoth's actual density could be as low as 250  $\text{kg m}^{-3}$ , so that what we observe today *is* representative of its primordial spin state. Our previous impact simulations on Ceres and Vesta (Mao & McKinnon, 2020) demonstrate (unsurprisingly) that the largest impacts dominate the angular momentum evolution of the target body; for Arrokoth, the formation of a single largest crater, such as Sky, could hypothetically change its spin, up or down, by a larger amount. We leave detailed investigation of Sky itself to Section 4. For now, we assume initially a comet-like density for Arrokoth of 500  $\text{kg m}^{-3}$ , and investigate the likelihood of a 30% angular momentum loss by impacts of small Kuiper belt objects. Because the critical rotation of Arrokoth's two lobes depends on its bulk density, by varying bulk density the likelihood of Arrokoth's ostensible despinning evolution changes accordingly (addressed in Section 3.3).

## 2.5. Initialization of Triaxial-Arrokoth's Impact Simulation

From a rotational dynamics point-of-view, the moment-of-inertia (MOI) and cross-sectional area are two key quantities in calculating the change in angular velocity after a given impact on TA (Equation 3 in Section 3.1). The principal MOI from the *New Horizons* Arrokoth shape model are  $(1.67, 7.23, 8.21) \times 10^{23} \times (\rho/250 \text{ kg m}^{-3}) \text{ kg m}^2$  (Keane et al., 2020). For our triaxial-Arrokoth model with semi-major axes (18.0, 9.1, 4.8) km, however, for a given density its principal MOI generally cannot simultaneously match the respective MOI of Arrokoth itself. Thus, we scale TA's density by  $619 \times (\rho/500 \text{ kg m}^{-3}) \text{ kg m}^{-3}$ . Adjusting the density has only a slight effect on crater and ejecta scaling (e.g., Equation 1), but critically, the rotational dynamics for TA are equivalent to what the actual Arrokoth would experience.

To summarize, our first simulations adopt a dynamically equivalent triaxial ellipsoid (TA) to represent the true bilobate Arrokoth with an initial spin of  $P = 11.26 \text{ hr}$ , and allows for a suite of 100 impactors (76% and 24% from the cold and hot classical KBO subpopulations, respectively) from small KBOs in the diameter range from 10 m to 1 km to collide with the modeled TA. We then vary certain parameters (e.g., impactor size range, KBO size-frequency differential slope, and Arrokoth bulk density) for further investigations in Section 3.



### 3. Results and Discussion

With 100 impacts in a given simulation, we group 5000 simulations as a Monte Carlo suite for better statistics on Arrokoth's spin evolution and final spin distribution after these impacts. In all our simulations we assume the impactor density to be identical to that of the target (e.g., TA). For each impact we also evaluate the porous asteroid disruption criterion from Equation 6 in Holsapple and Housen (2019) to test for potential catastrophic events.

#### 3.1. Impact Processes—A Process of Mass Loading and Ejecta Loss

In our previous work (Mao & McKinnon, 2020), we obtained a general analytical formula for the change in angular velocity ( $\delta \vec{\omega}$ ) after a given impact onto an asteroid and subsequent ejecta loss,

$$\delta \vec{\omega} = (I + \Sigma \delta I)^{-1} \cdot [m \vec{r} \times \vec{V} - \delta \vec{L}_{\text{ej}} - (\Sigma \delta I) \cdot \vec{\omega}], \quad (3)$$

where  $I$  is the asteroid's MOI (in full tensor form),  $\Sigma \delta I$  is the total change in Arrokoth's MOI from  $(\Sigma \delta I)_{ij} = (m - m_{\text{ej}}) (\vec{r}_i \delta_{ij} - r_i r_j)$ , where  $\delta_{ij}$  is Kronecker delta,  $m$  and  $m_{\text{ej}}$  are respectively the impactor and the lost ejecta mass,  $\vec{r}$  is the coordinate of impact location in the body-fixed frame,  $\vec{V}$  is the velocity vector,  $\vec{\omega}$  is pre-impact angular velocity, and  $\delta \vec{L}_{\text{ej}}$  is the angular momentum lost to escaping ejecta, following the azimuthal dependence in Richardson (2011) (see Equation 5 in Mao & McKinnon [2020]). We assume principal axis rotation of TA and thus diagonalize the moment tensor after each impact (see techniques described in Henych & Pravec, 2013); we will come back to discuss damping of non-principal axis rotation induced by impacts in Section 4.4.

For our first simulations, Figure 3 is the plot of all the individual runs combined. In the top panel (Figure 3a), each colored curve is a simulated spin evolution of Arrokoth from  $P = 11.26$  hr. With the maximum possible impactor diameter set at 1 km, and a probability distribution for impactor size given by  $dN(d) = [0.75 d^{-1.75} / (d_{\text{min}}^{-0.75} - d_{\text{max}}^{-0.75})]$  (Section 2.3), the expected or mean value of  $d$  over the interval 10 m to 1 km is 67 m. Thus, we anticipate that the majority of the simulated impactors do not affect TA's spin much. Only stochastic outliers, that is, large impacts, in general can change TA's spin substantially.

Spin evolution curves and the final distribution of spin states in Figure 3 show that the majority of the simulations, about 86%, end close to the original spin value, within  $11.2 \pm 0.6$  hr ( $1\sigma$ ), with an interquartile range (IQR) from 11.0–11.3 hr. Spin evolution is characterized by a combination of wide “plateaus” with a handful of “jumps,” the latter generally caused by large impacts (Figure 3a). Because of the stochastic nature of the large impacts, Arrokoth's final spin may increase or decrease. About 10% of the time Arrokoth's entire spin evolution stays on one side of 11.26 hr after the first impact in the simulation. It is common for Arrokoth (or asteroids in general) to have its spin change fluctuate with respect to the initial spin, although it becomes increasingly unlikely with time that Arrokoth crosses its initial spin multiple times. Considering the final spin distribution of TA after these 100 impacts, a Lorentzian is used to fit the results (Mao & McKinnon (2020) found this function to be appropriate). Incorporation of  $\sim 24\%$  hot classical helps extend the span of the final spin distribution, to 6-to-23 hr (compare with the results shown in Mao et al., 2020a). Using 15.92 hr as a benchmark to assess whether or not 30% angular momentum loss is met, only 0.04% of the simulations meet this goal. However, if we explicitly use angular momentum as the criterion, 0.3% of the time Arrokoth's final angular momentum is 30% less (the subtle difference has to do with Arrokoth's mass changing as it is bombarded). Regardless, we find that the likelihood of Arrokoth's spin period increasing by more than 4.5 hr to be exceedingly small.

We also track potential disruption events in the simulation, while noting that our simulations are based on the surviving cratering record on Arrokoth (i.e., no reassembly or resurfacing processes owing to disruption). Combining Equation 6 in Holsapple and Housen (2019) with its velocity dependence made explicit, the energy threshold per unit target mass ( $Q_d^*$ ) to break a porous asteroid and have it lose at least half its mass is given by

$$Q_d^* = \left[ 2 \times 10^3 R^{-0.25} + 4 \times 10^5 \left( \frac{R}{5 \times 10^5} \right)^{1.23} \right] \left( \frac{V_{\perp}}{3.89 \times 10^3} \right)^{0.6} \text{ J kg}^{-1}, \quad (4)$$

where  $R$  is the spherically equivalent radius of the asteroid in meters and  $V_{\perp}$  is the vertical component of the impact velocity in  $\text{m s}^{-1}$ . For a typical  $45^\circ$  impact at  $300 \text{ m s}^{-1}$  and TA's average radius of 9.3 km,  $Q_d^* \approx 560 \text{ J kg}^{-1}$ .

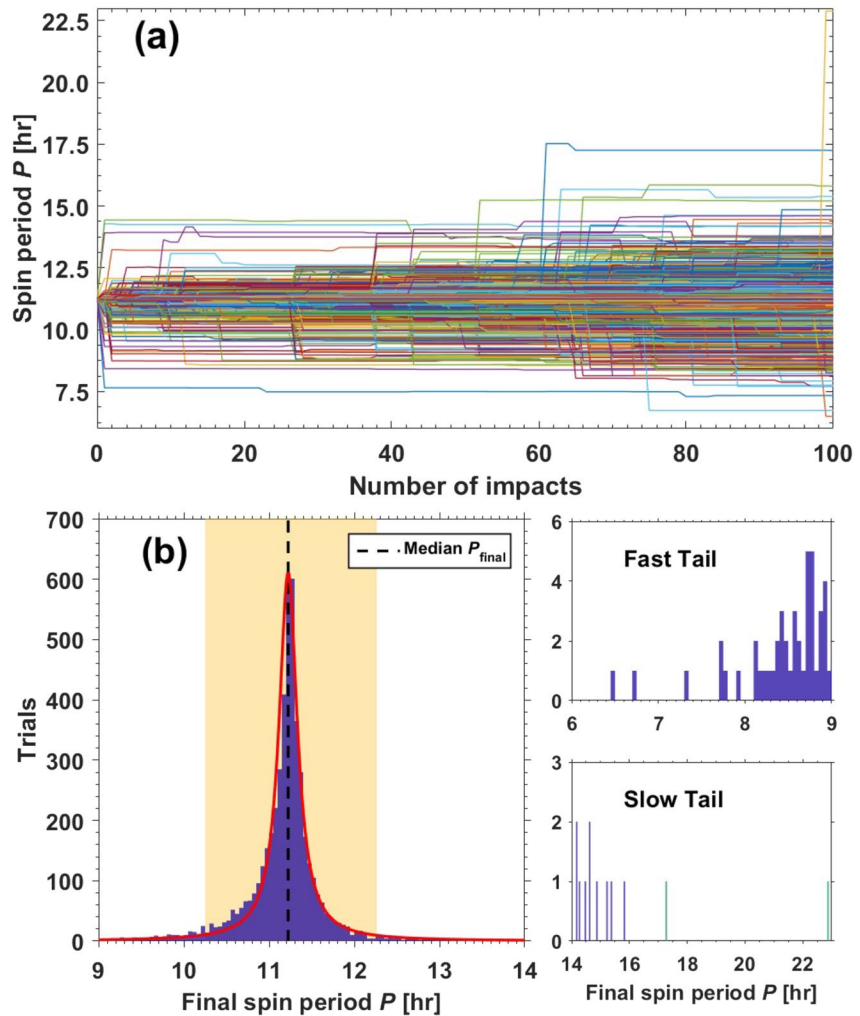


**Figure 3.** (a) Arrokoth simulated spin evolutions stacked together from the initial simulation ( $500 \text{ kg m}^{-3}$  bulk density), 5000 curves in total, with each colored curve a specific run started at  $P = 11.26 \text{ hr}$ . All sharp changes in spin are caused by large impacts. (b) Final spin distribution. The range of final spins is  $6.5\text{--}22.9 \text{ hr}$ . The shaded region denotes  $11.26 \pm 1 \text{ hr}$ , with 93% of Arrokoth's final values within this region. The red curve is a Lorentzian fit for a median value of  $11.22 \text{ hr}$  and an interquartile range =  $11.03\text{--}11.34 \text{ hr}$ . Expanded views of extreme outcomes are shown on the right, with two runs highlighted in green, where Arrokoth has slowed down to its observed spin period or longer.

Under this condition, assuming an impactor with  $d = 1 \text{ km}$  and  $\delta = 500 \text{ kg m}^{-3}$ , the specific kinetic energy imparted onto TA is only about  $3 \text{ J kg}^{-1}$ , far less than the threshold. This specific set of impact parameters corresponds to the largest size crater (Sky) observed on Arrokoth (Figure S1 in Supporting Information S1). We also calculate the respective  $Q_d^*$  value for a spherically equivalent Small Lobe, that is,  $\sim 1/3$  the volume of TA. Our results indicate that TA, as well as Arrokoth's individual lobes always survive against disruption in our initial model, as is generally the case in the cold classical region (Abedin et al., 2021).

These first simulation results reconfirm the survival of Arrokoth during its impact history. More importantly, our results imply that, if Arrokoth has a comet-like bulk density and only experiences impacts from small classical KBOs since lobe merger, it is highly unlikely for it to have undergone the required angular momentum loss and have its spin reduced to the observed value today. Similarly, it is reasonable to infer that if impact is the *only* secular mechanism affecting Arrokoth's spin dynamics, then what we observe today may be representative of the unperturbed, primordial spin of Arrokoth (at least post the nebular era, when gas drag may have been important (McKinnon et al., 2020; Lyra et al., 2021)).

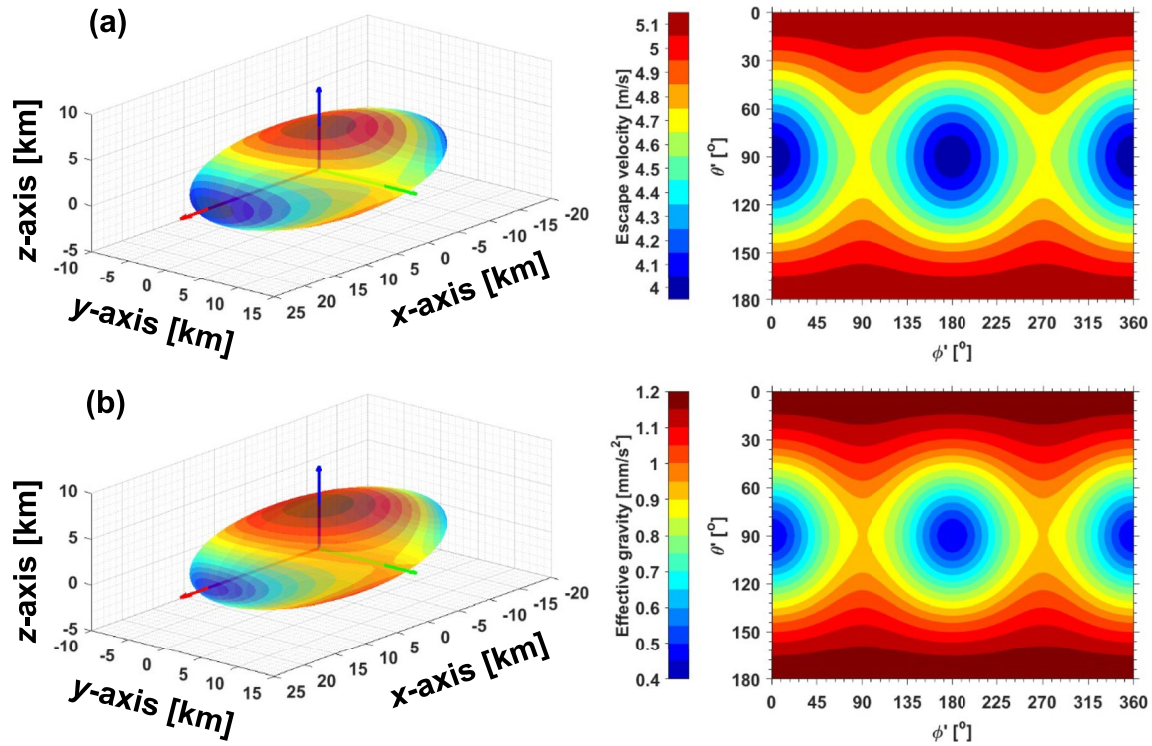


**Figure 4.** Gravity and escape velocity at the surface of the modeled triaxial-Arrokoth. (a) Escape velocity for a non-rotating triaxial ellipsoid as a function of  $\phi'$  (longitude) and  $\theta$  (parametric colatitude, see Figure S2 in Supporting Information S1). We assume  $\rho = 500 \text{ kg m}^{-3}$ . Escape velocity is lowest at the tips of the longest principal axis ( $\sim 4 \text{ m s}^{-1}$ ) and is highest at the poles ( $\sim 5.1 \text{ m s}^{-1}$ ). (b) Effective gravity corresponding to rotation period of 11.26 hr and  $\rho = 500 \text{ kg m}^{-3}$ . Effective gravity is derived from the triaxial ellipsoid gravitational potential (MacMillan, 1930) combined with centrifugal acceleration. Pattern is similar to that of escape velocity, with minimum and maximum values of  $4.8 \times 10^{-4} \text{ m s}^{-2}$  and  $12 \times 10^{-4} \text{ m s}^{-2}$ , respectively.

### 3.2. Granular Material – (Almost) Losing Mass all the Time

We use mass-velocity scaling (Housen & Holsapple, 2011) in the gravity regime to calculate the amount of ejecta that escapes Arrokoth after a given impact

$$\frac{m_{ej}(> V_{esc})}{m} = \frac{3k}{4\pi} \left( \frac{C_1 V'_\perp}{V_{esc}} \right)^{3\mu} \left( \frac{\delta}{\rho} \right)^{3\nu-1}, \quad (5)$$

where  $m_{ej}(> V_{esc})$  is the mass of ejecta with speed greater than the escape speed  $V_{esc}$  at the impact location (see Figure 4 for additional details),  $k = 0.3$ ,  $C_1 = 0.55$ ,  $\mu = 0.41$ , and  $\nu = 0.4$  are scaling parameters from Housen and Holsapple (2011) for regolith-like, granular materials, and  $V'_\perp$  denotes the vertical component of the impact velocity in the rotating frame. Escape velocity on TA (see Table 1 for parameters) varies from  $4 \text{ m s}^{-1}$  to  $5.1 \text{ m s}^{-1}$ , and is lowest near the  $a$ -axis, and highest at the poles (Figure 4).

Because the typical impact speed is at least two orders of magnitude greater than the escape velocity, the potential for impact erosion is great even if Arrokoth is highly porous, which normally favors net mass accumulation. For example, for a typical cold classical KBO with impact speed of  $300 \text{ m s}^{-1}$  at an impact angle of  $45^\circ$ , the ejecta that is lost to space is  $\sim 3$  times the mass of the impactor. As the impact speed increases (i.e., for typical impact speeds of hot classical KBOs), so does the amount of escaped ejecta. Only at very low impact velocities or very oblique impact angles does this mass ratio drop below 1 (i.e., Arrokoth accumulates mass). The actual scenario is somewhat more complicated, however, because the impact point moves with Arrokoth's rotational velocity (the projection of  $\vec{\omega} \times \vec{r}$  on the local east direction), so that ejecta more easily escapes to the local east (see Dobrovolskis & Burns, 1980, 1984). Our initial results indicate that Arrokoth almost always experiences mass loss after 100 impacts (only 2 simulations out of 5000 ended with Arrokoth gaining mass). Figure 5 is a histogram of the distribution of the ratio of integrated ejecta lost to total impactor mass. The mean of this ratio is  $9.3 \pm 8.6 (1\sigma)$ .



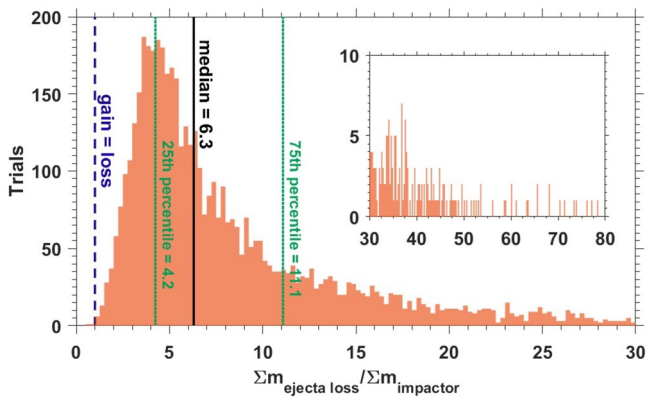


**Figure 5.** Histogram of the ratio of total lost ejecta mass to the integrated impactor mass from our initial simulation. The results are positively skewed with a skewness factor of 2.9. Arrokoth loses mass in >99.9% of the simulations, if cratering there follows porous, regolith-like gravity-regime scaling (Housen & Holsapple, 2011). Statistically, about 0.15% of Arrokoth's initial mass has likely been lost during its observable impact history. Inset shows the distribution of this ratio at the higher end (note different vertical axis scale).

This number translates to a modest mass loss of  $0.15 \pm 0.19$ – $0.15\%$  ( $1\sigma$ ) of Arrokoth's initial mass, a testament to the benign impact environment in the cold classical Kuiper belt (at least since the end of the era of giant planet migration or somewhat later (Morbidelli et al., 2021)).

### 3.3. On Arrokoth's Density

Our initial simulation suite fixed Arrokoth's bulk density (for the purpose of computing its MOI) at  $500 \text{ kg m}^{-3}$ . The required angular momentum loss, if Arrokoth evolved from a synchronous rotation state to its observed spin, is 30%, as discussed in Section 2.4. Because of the  $\rho^{-0.5}$  dependence of the synchronous rotation rate (Equation 2), a lower bulk density means a slower critical rotation, requiring less angular momentum loss to reach Arrokoth's present-day spin. For example, if Arrokoth's density is  $300 \text{ kg m}^{-3}$ , then a less stringent  $\sim 9\%$  angular momentum loss would be adequate to explain its current spin, due to impacts alone. Indeed, angular momentum loss in the 5%–10% range is not unreasonable; both Ceres (Mao & McKinnon, 2020) and Vesta (Fu et al., 2014) have been proposed to have been spinning faster in the past by nearly 7% and subsequently despun by large impacts. In order to address how bulk density affects the likelihood of Arrokoth's ostensible despinning history (via impacts), we ran additional suites of simulations by varying Arrokoth's bulk density from  $250 \text{ kg m}^{-3}$  (the minimum plausible for rotational stability) to  $450 \text{ kg m}^{-3}$ .

We list simulation results in Table 2 with corresponding boxplots of final spin distributions in Figure 6. Unless Arrokoth has a very low density (i.e., close to  $250 \text{ kg m}^{-3}$  to begin with), the probability of its despinning from initial synchronous rotation to its present-day value due to impacts is only a few percent at best. Most notable from these results is that the IQRs from each simulation suite span no more than  $\sim 0.6$  hr, regardless of bulk density.

Technically the lowest density we explore,  $250 \text{ kg m}^{-3}$ , actually implies a somewhat higher likelihood of observing a *faster* spin than the initial 15.92 hr critical rotation after 100 impacts, owing to the geometry of large-impact angular momentum vector addition (Mao & McKinnon, 2020). In fact, all simulations run show a modest tendency towards spinup from the initial rotation rate, whatever it may be, for the same reason.

**Table 2**  
Simulation Results Varying  $d_{\text{max}}$  and Arrokoth Bulk Density

		$\rho_{\text{Arrokoth}}$ [ $\text{kg m}^{-3}$ ]	250	300	350	400	450	500
		Corresponding critical rotation [hr]	15.92	14.53	13.45	12.59	11.87	11.26
SFD from Singer, Spencer et al. (2019)	$d_{\text{max}} = 1 \text{ km}$	37.58% [15.41–16.04]	2.02% [14.14–14.65]	0.84% [13.13–13.56]	0.20% [12.32–12.69]	0.08% [11.63–11.95]	0.04% [11.03– 11.34]	
	$d_{\text{max}} = 2 \text{ km}$	28.42% [12.36–15.99]	7.50% [11.75–14.59]	3.98% [10.99–13.54]	2.34% [10.39–12.67]	1.60% [10.13–11.95]	1.00% [9.62– 11.34]	
SFD from Morbidelli et al. (2021)	$d_{\text{max}} = 1 \text{ km}$	44.60% [15.92–15.92]	0.10% [14.53–14.53]	0.06% [13.45–13.46]	0.02% [12.59–12.59]	0.00% [11.87–11.87]	0.00% [11.26– 11.26]	
	$d_{\text{max}} = 2 \text{ km}$	44.10% [15.92–15.92]	0.28% [14.53–14.53]	0.18% [13.45–13.46]	0.12% [12.59–12.59]	0.06% [11.87–11.87]	0.06% [11.26– 11.26]	

*Note.* Probabilities that Arrokoth's final spin period exceeds today's value after 100 impacts are shown. Square brackets denote the interquartile range (IQR) of the final spin period distribution from each suite, in hr. When catastrophic disruption occurs, we consider the pre-disruption spin as the final spin for that particular run, though no such disruptions were found for  $d_{\text{max}} = 1 \text{ km}$ ; for  $d_{\text{max}} = 2 \text{ km}$ , the disruption probabilities are  $\sim 2\%$ – $3\%$  for the Singer, Spencer et al. (2019) size-frequency distribution (SFD) and  $<0.1\%$  for the Morbidelli et al. (2021) SFD. For the latter SFD, the IQR ranges are extremely narrow.

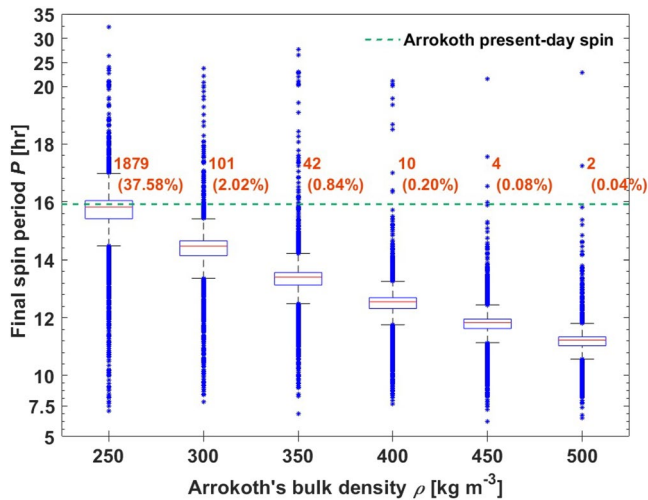


**Figure 6.** Boxplots of simulation results varying Arrokoth's bulk density from  $250 \text{ kg m}^{-3}$  to  $500 \text{ kg m}^{-3}$ . Each boxplot is the compilation of 5000 simulation runs, referred to as a suite. Red lines are the median values from each suite, box height is the IQR, and the whisker length, extending from the top and the bottom of a given box, is  $1.5 \times \text{IQR}$ . All the blue symbols are statistically considered as outliers for Lorentzian fits. Numbers and probability values above the dashed green line (Arrokoth's observed spin), are the total simulations in which Arrokoth's final spin after 100 impacts is slowed down to 15.92 hr or more and the corresponding percentage of the suite, indicating the ineffectiveness of angular momentum evolution by collisions with small KBOs. As Arrokoth's density approaches  $250 \text{ kg m}^{-3}$ , it is easier for its spin to obtain the present-day observed value by impacts alone.

### 3.4. Different Size-Frequency Differential Slope for Small KBO And/ Or Larger Impacts?

A recent reassessment of the KBO SFD by Morbidelli et al. (2021) argues for a relatively steeper SFD differential slope over the size range in which we are interested: the respective log  $dN$  slopes are  $-4$  for  $d \lesssim 30 \text{ m}$  and  $-2.2$  for  $d$  from  $30 \text{ m}$  to  $2 \text{ km}$ . Steeper SFD slopes downplay the importance of larger impacts. Probabilistically speaking, the chance of randomly picking a large (i.e., Sky-forming) impact diminishes rapidly as the log SFD slope steepens. To compensate, we allow for a larger upper bound for the maximum impactor size  $d_{\text{max}}$ . We thus conducted a series of simulations with the two different SFD models, from Singer, Spencer et al. (2019) and Morbidelli et al. (2021), and  $d_{\text{max}}$  of  $1$  and  $2 \text{ km}$ . Larger impactors, if fast and non-oblique, have a greater potential to cause catastrophic disruption of TA, or indeed the individual lobes of Arrokoth, but we still find this to be an unlikely model outcome (though not entirely ruled out).

The cumulative results of alternate SFD slopes with different values for  $d_{\text{max}}$  are summarized in Table 2. Comparing results with the Singer, Spencer et al. (2019) SFD but with different  $d_{\text{max}}$ , it is clear that the expansion of impactor size range has significant effects. The chances of Arrokoth achieving its present-day spin through impacts increases for all of the bulk densities tested. Even though the average impactor size ( $\sim 84 \text{ m}$ ) does not change much (cf.  $\sim 67 \text{ m}$  when  $d_{\text{max}} = 1 \text{ km}$ ), there is a  $\sim 1.3\%$  of chance of an impactor  $d > 1 \text{ km}$  in a given simulation. As impactor angular momentum scales as  $d^3$ , Arrokoth's spin angular momentum inevitably should be disturbed more, compared with our original simulations. Another noticeable feature is the enlarged IQR of the final spin, with a spin-up tendency (i.e., more simulations end with spin periods shorter than the initial synchronous rotation in each suite).

In comparison, for the Morbidelli et al. (2021) SFD, the probability of Arrokoth despinning from synchronous rotation to its present-day spin state is exceedingly unlikely, irrespective of whether  $d_{\text{max}}$  is  $1$  or  $2 \text{ km}$ . Only if the bulk density is low to begin with and the original synchronous rotation rate quite similar to Arrokoth's present value, is impact despinning plausible, though this is obviously a trivial conclusion.

## 4. Sky-Forming Impact

The modeling above is based on Arrokoth's observed crater density, but because observations of its non-encounter side were sparse (Spencer et al., 2020), it is generalized so that a full spectrum of possible impact histories consistent with Arrokoth's surface geology could be explored. Specifically, the global cratering history on Arrokoth is not known, as opposed to, say, the situation at Ceres or Vesta. Because Sky is such a dominant impact feature on Arrokoth, however, it is worthwhile to examine likely aspects of its formation alone, from an angular momentum perspective. This serves to give a measure of its possible effects, and which might be doubled (e.g.,) if one imagines there might be a similar-sized impact on the unilluminated, non-encounter side. Moreover, Sky's location on the leading side of the Small Lobe, far from Arrokoth's center-of-mass, is well positioned to slow Arrokoth's spin, and so needs to be explicitly modeled. To do so, we adopt a more directly applicable bilobate geometry for Arrokoth, and constrain the specific characteristics of the Sky-forming impact.

### 4.1. Determining the Sky Crater Impactor Size and Velocity

From stereo topographic analysis, Schenk et al. (2021) found the diameter and depth of Sky (with respect to a reference triaxial ellipsoid for the Small Lobe) to be close to  $7$  and  $0.85 \text{ km}$ , respectively. We note the diameter of Sky determined in Spencer et al. (2020) is somewhat smaller,  $\sim 6.35 \text{ km}$ , but we retain the larger number as a limiting value (nor does this minor difference affect the analysis below). The volume of Sky ( $V$ ) can then be approximated by a spherical cap geometry, which yields  $\sim 16.7 \text{ km}^3$ . Following point-source,  $\pi$ -group scaling, the

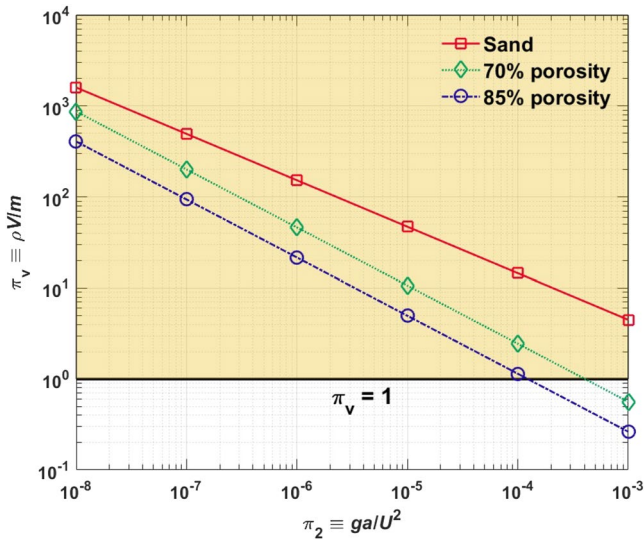


**Figure 7.** Cratering efficiency comparison between regolith (dry sand) and highly porous granular materials in the gravity regime (from Housen et al., 2018). Smaller craters on Arrokoth (low  $\pi_2$ ) are likely affected by material strength, even for low comet-like strength values of 1 kPa, but Sky (with a typical  $\pi_2 \sim 0.5\text{--}1 \times 10^{-5}$ ) is large enough to have formed in the gravity regime. Point-source scaling is not applicable too close to the impactor (see discussions in Housen et al., 2018 and Singer et al., 2013), so we restrict our Monte Carlo simulations to  $\pi_v > 1$ .

classic cratering efficiency  $\pi_v \equiv \rho V/m$ , where  $m$  the impactor mass, can be calculated immediately for a given impact.  $\pi_v$  is related to the gravity-scaled size  $\pi_2 \equiv ga/U^2$ , where  $g$  is the effective gravity at the impact location,  $a$  is impactor radius, and  $U$  is again the vertical component of the impact velocity.

To model the Sky-forming impact, we first select an impactor size and vertical impact speed, drawing from the velocity distribution (Figure 2) and the KBO SFD. Gravity scaling (equivalent to Equation 1; see Singer et al., 2013) then gives an estimated crater  $V$ . If this value is within 10% of  $16.7 \text{ km}^3$ , we accept this combination of impact parameters as possible for Sky. This process is then repeated many times to get a statistical picture of Sky's likely formation conditions. To allow for very large, slow, or highly oblique impactors, we further relax the upper limit  $d_{\text{max}}$ , setting the upper bound at 7 km (larger sizes would make little sense for a 7-km wide crater). Following the KBO SFD log slopes estimated in Singer, Spencer et al. (2019), we adopt a slope of  $-3$  for impactors with diameters from 2 to 7 km, while the differential slope for smaller impactors ( $-1.75$ ) is unchanged from above.

A more sophisticated (if less certain) crater scaling is possible for Sky, and Arrokoth generally, one that explicitly takes into account the roles of high bulk porosity and possible compaction of highly porous materials (Housen et al., 2018). Even the maximum Arrokoth bulk density in our modeling implies a rather large porosity for plausible rock- and organic-matter-bearing bodies of the Kuiper belt (Bierson & Nimmo, 2019; Grundy et al., 2020; Lisse et al., 2021; McKinnon et al., 2017), perhaps 70%–75%. Such porosities are consistent with estimates for comet 67P (70%–80%, Groussin et al., 2019). In comparison, the scaling used in Greenstreet et al. (2019) is based on experimental results summarized in Holsapple (1993) and Housen and Holsapple (2011), for unconsolidated sand- or regolith-like materials that have “normal” porosities closer to 30%–40%.

The role of compaction, or crush up of pre-existing porosity, is less clear for Arrokoth, and will be the subject of a future paper (cf. McKinnon et al., 2021 for a preview). Figure 20 in Housen et al. (2018) predicts, nominally, that compaction cratering may *not* be important for Arrokoth. But, high porosity can have important effects in the gravity regime even without, or with minimal, crater growth by compaction. These authors proposed a new crater scaling for highly porous granular materials (those with porosities  $n$  greater than 50%), which in the gravity regime and for equal impactor and target densities ( $\rho = \delta$ ) simplifies to

$$\pi_v = 0.023 \pi_2^{-3\mu/(2+\mu)} \times \text{psf}(n) \quad (6)$$

$\mu$  in this case is taken to be 0.54 and  $\text{psf}(n) = 10.4 \exp(-5.07n)$  is an empirical porosity scale factor derived by Housen et al. (2018) from centrifuge impact experiments. For Arrokoth we assume that  $n$  varies linearly from 0.70 to 0.85 for bulk densities between 500 and 250  $\text{kg m}^{-3}$ , respectively. This scaling is illustrated in Figure 7.

#### 4.2. Bilobate Geometry

Because the location of Sky crater is far from the neck region (see the shape model in Figure 1), mathematically it is easier to calculate the angular momentum carried away by escaped ejecta. Furthermore, in the extreme of compaction cratering where no ejecta is lost at all, spin evolution becomes a simple matter of vector addition of incoming angular momentum. For these reasons, we proceed to a more accurate representation of Arrokoth by using its best-fit bilobate shape as two triaxial ellipsoids (Spencer et al., 2020), with major axis lengths for the Large Lobe (20.6, 19.9, 9.4) km and for the Small Lobe (15.4, 13.8, 9.8) km (see Figure 8).

For this model, we assume both lobes are perfectly aligned, and their centers of mass are separated by 17.2 km (Keane et al., 2020). From the shape model, the lowest point within Sky crater is found, with the corresponding impact point on the Small Lobe triaxial ellipsoid (Figure 8). With both triaxial ellipsoid gravitational potentials

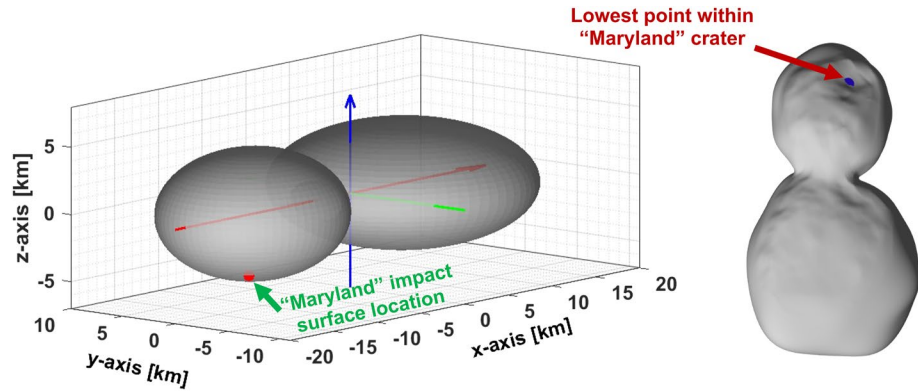
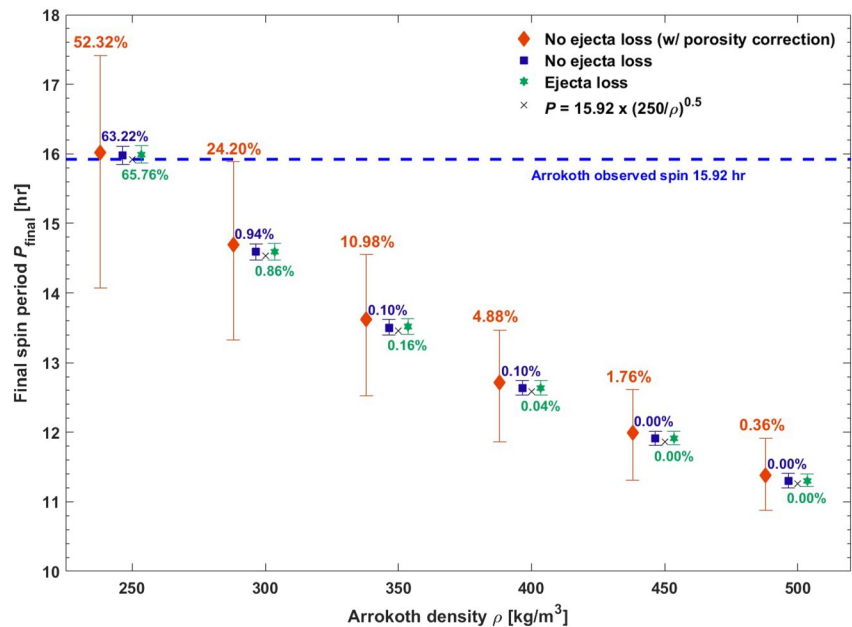


**Figure 8.** Bilobate model for Arrokoth. Colored arrows are principal axes of Arrokoth (red for  $a$ -axis, green for  $b$ -axis, and blue for  $c$ -axis). To be consistent with the coordinate system in the shape model,  $+z$  direction is the spin angular velocity. The red dot is the impact point. A vector perpendicular to the local surface, directing into the Small Lobe, passes through the lowest point within Sky ("Maryland") (blue dot on the right).

and gravity (MacMillan, 1930), we calculate the effective gravity at the impact location to be  $\approx 0.8 \text{ mm s}^{-2}$  for a bulk density of  $500 \text{ kg m}^{-3}$  and spin period of 11.26 hr. Similarly, the escape velocity can be derived and used to determine escaped ejecta mass.

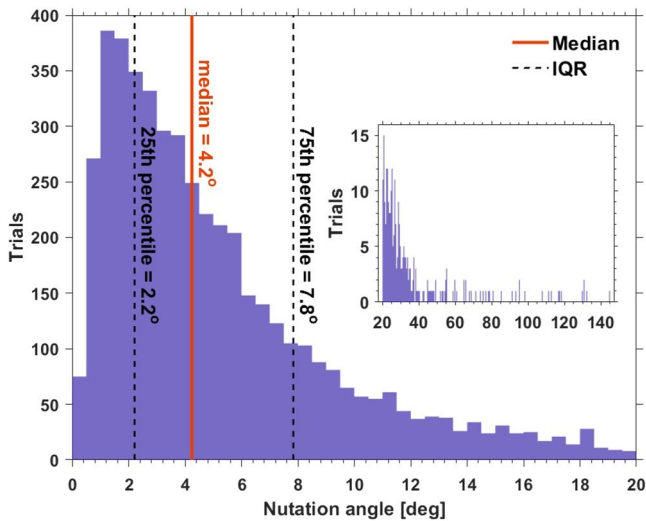
### 4.3. Simulation Results and Comparisons

Figure 9 shows the compiled distributions from each simulation suite, grouped by assumed Arrokoth (and impactor) density and whether or not ejecta is retained or allowed to escape. Different from the boxplot in Figure 6, here we use the error-bar to denote the the IQR of Arrokoth's final spin after the formation of Sky without adding



**Figure 9.** Comparisons of Sky simulation results with and without ejecta loss and porosity scaling. Colored symbols (diamond, square, hexagram) are the median values of simulation suites with 5000 Monte Carlo impacts, grouped by assumed bulk density and whether or not porosity scaling is included. Each set with its associated cross corresponds to the same  $\rho$ , with horizontal offsets for clarity. Error bars span the IQR of the results. Percentage values are, as in Figure 6, the probability of Arrokoth's ostensible despinning realized by the formation of Sky. Compared with results in Figure 6, Sky's formation alone is insufficient to cause Arrokoth's spin to so change, but has a much greater overall effect when porosity scaling is included.





**Figure 10.** Histogram of nutation angle from Sky impact simulations in Figure 9 (porosity scaling included but all ejecta retained,  $\rho = 500 \text{ kg m}^{-3}$ ). While the range is large, from  $0^\circ$  to  $145^\circ$ , the majority of the nutation angles are only a few degrees (e.g., 7%  $< 1^\circ$ , 91%  $< 15^\circ$ ). The timescale for Arrokoth to return to principal axis rotation is generally short (Section 4.4).

points outside of the IQR. Each colored symbol is the median value from a given simulation suite and the respective colored numbers are the likelihood of Arrokoth's post-impact spin period achieving today's value or longer. For traditional, regolith gravity scaling from Figure S1 in Supporting Information S1 (green and blue symbols in Figure 9), as Arrokoth density decreases from  $500 \text{ kg m}^{-3}$ , the likelihood that its post-impact spin slowed to 15.92 hr increases, a similar trend to that observed from simulations with 100 impacts of varying sizes but with consistently twice the likelihood (except of course at  $\rho = 250 \text{ kg m}^{-3}$ ) (Table 2). This finding justifies our systematic investigation of Sky's formation, because the collective effects from the numerous smaller impacts on Arrokoth's spin tend to cancel out.

Results are essentially the same when ejecta escape is suppressed (blue symbols in Figure 9). We found that across the six suites of simulations, the total mass loss due to Sky's formation is less than  $\sim 0.03\text{--}0.04\%$  of Arrokoth's mass; dynamically speaking, the lost ejecta does not carry away much angular momentum, as most ejecta moves at speeds closer to escape speed rather than at the impactor's original speed. Because of Sky's position on Arrokoth, however, its formation tends to slow down Arrokoth's spin, and it can be seen from Figure 9 that both blue and green symbols are above the critical rotations corresponding to specific density values (crosses), although the effect is not pronounced.

Results are quantitatively different when the porosity scale factor (psf) is included (red symbols in Figure 9). Because of a reduction in crater efficiency (i.e., by 0.3 for 70% porosity), larger impactors are required to create Sky, all other things being equal. This substantially broadens the IQR range of the resulting spins, and significantly increases the number of possible outcomes for which Arrokoth may be slowed from synchronous to a 15.92 hr rotation. Moreover, the reduction in crater efficiency is more pronounced for lower densities, so the IQR range expands accordingly. From a statistical point of view, such a slowing cannot be rejected at the 95% confidence level for Arrokoth densities  $\lesssim 400 \text{ kg m}^{-3}$ .

Arrokoth's post-impact linear momentum may be greater than that introduced by the incoming impactor due to ejecta recoil; the measure of the ratio of the linear momentum added to that carried by the impactor is a transfer factor called  $\beta$  (e.g., Holsapple & Housen, 2012; Cheng et al., 2020), and one of the objectives of NASA's DART mission includes an accurate determination of  $\beta$  through a controlled kinetic impact on the Didymos system (Cheng et al., 2020). We do not examine  $\beta$  here in any detail, but do briefly comment later on (in Section 5).

We note that the formation of Sky may have had other dramatic effects on Arrokoth. Hirabayashi et al. (2020) argue that its formation may have caused the neck to fail and the two lobes to grossly rearrange. While we do not necessarily disagree, we point out that there is no particular evidence in *New Horizons* images for such a rearrangement, plus such considerations are rather beside the point for our principal interest, the possible change in Arrokoth's spin angular momentum. We will consider the splitting of Arrokoth in greater detail in a future paper.

#### 4.4. Non-Principal Axis Rotation and Its Rapid Damping

The "giant" Sky-forming impact not only brought in substantial angular momentum, but also induced a significant change in Arrokoth's moment-of-inertia tensor. Even with principal axis rotation initially (i.e., no angular offset between spin axis orientation and the shortest principal axis), after the collision the angular momentum vector does not necessarily coincide with the orientation of the maximum MOI. The angle between these two vectors is historically defined as the nutation, or wobble, angle (Burns & Safronov, 1973). We show an example of nutation angle histogram from simulation results with porosity scaling included (red symbols in Figure 9) and  $\rho = 500 \text{ kg m}^{-3}$  (Figure 10). The median nutation angle is  $4.2^\circ$  and 91% of the time it is less than  $15^\circ$ , a cutoff value over which the nutation phase can be photometrically observed from the light curve for a small body (Henych & Pravec, 2013).

Making the logical assumption that Sky formed early in Arrokoth's history (see surface age discussion in Spencer et al., 2020), but that its formation did not precede lobe merger (Lyra et al., 2021; McKinnon et al., 2020), could



the induced nutation have lasted long enough to be seen by *New Horizons*? Today, the maximum principal MOI of Arrokoth is essentially aligned (to within  $0.4^\circ$ ) with Arrokoth's spin axis, based on the shape model (Keane et al., 2020). Thus, either Arrokoth acquired a very small nutation angle (e.g.,  $<1^\circ$ ), or more likely, any non-principal axis rotation has long damped.

In Burns & Safronov (1973), the damping time ( $\tau_{\text{damp}}$ ) of a small body is given by

$$\tau_{\text{damp}} \sim \mu^* Q / (\rho K R^2 \omega^3), \quad (7)$$

where  $\mu^*$  is the rigidity of Arrokoth (that for solid water ice is 3.5 GPa; Petrenko & Whitworth, 2002),  $Q$  is tidal quality factor (assumed to be 100; see Goldreich & Soter, 1966),  $K$  is a parameter equal to  $0.1 \times \left(1 - \frac{A+B}{2C}\right)^2$ , with  $A < B < C$  being the principal MOI of Arrokoth,  $R$  is the average radius, and  $\omega$  is the angular speed. With the bilobate representation of Arrokoth in the model,  $\tau_{\text{damp}} = 3.5 \times (500 \text{ kg m}^{-3}/\rho)^{2.5} \times (Q/100) \times (\mu^*/3.5 \text{ GPa})$  Myr (note that we are including the dependence of synchronous  $\omega$  on  $\rho$  in this estimate). Even if Arrokoth's bulk density is  $250 \text{ kg m}^{-3}$ , within  $\sim 20$  Myr the excess wobble energy should dissipate, and on a time scale much less than the age of the Solar System. In addition, both the  $\mu^*$  and  $Q$  adopted above are almost certainly upper bounds. The rigidity of Arrokoth should be much smaller than that of solid water ice, due to its likely high porosity, and  $Q$  may be smaller than the nominal value of 100 as well (see Goldreich & Sari, 2009). Goldreich and Sari (2009) derive for a highly porous, granular body (rubble pile) an order-of-magnitude estimate for its effective rigidity,  $\gtrsim \text{few} \times (\rho g R \mu^*)^{1/2}$ . For Arrokoth this limiting value is  $\sim 20$  MPa. Thus, Arrokoth likely returns to principal axis rotation within a few tens of kyr after any given impact. Such rapid damping justifies our implicit assumption of principal axis rotation between impacts in the triaxial Arrokoth modeling (Section 3), as this timescale is much shorter than the average time interval between the impacts in our model ( $\sim 40$  Myr).

## 5. Conclusions

We adapted our Monte Carlo impact model, originally developed for Ceres and Vesta (Mao & McKinnon, 2020), and which incorporates the dynamics of ejecta loss and associated momentum recoil, to investigate Arrokoth's possible spin evolution. Specifically, we tested whether impacts from small classical Kuiper belt objects could slow Arrokoth's spin from a presumed critical, synchronous rotation rate (dependent on assumed bulk density) to its presently observed spin period of  $\approx 15.9$  hr. We use a dynamically equivalent triaxial ellipsoid to represent bilobate Arrokoth. This geometry neglects the presence of the neck between the two lobes, a feature susceptible to potential failure after very large impacts (Hirabayashi et al., 2020), but this geometry serves our general purpose of investigating the angular momentum exchange between the impactors and Arrokoth over time.

In our initial simulations—100 impactors total, 76% from cold and 24% from hot classical KBOs, drawn from an impactor diameter range between 10 and  $10^3$  m to be consistent with Arrokoth's observed cratering record, and a bulk density for both impactors and Arrokoth of  $500 \text{ kg m}^{-3}$ —we find very modest effects. For over 90% of the trials, Arrokoth's spin cumulatively changes by less than 1 hr from its assumed initial 11.3 hr period, faster or slower, and the probability that its spin period was reduced to today's 15.9 hr is trivially small. We progressively varied model parameters to assess their effects. We tested bulk densities for Arrokoth (and its corresponding impactors) between  $250 \text{ kg m}^{-3}$  and  $500 \text{ kg m}^{-3}$ , an expanded impactor size range (up to 2 km), and different SFD log slopes for the impactor population. The effects on Arrokoth's spin angular momentum evolution, in a relative sense, are modest at best. The only parameter that really matters is bulk density, and then only because the initial synchronous rotation rate for lower bulk densities is closer to the present value, with the gap closing completely for  $\rho \approx 250 \text{ kg m}^{-3}$ . The inference we draw from these detailed calculations is that spin evolution from impacts over time is unlikely to have been important for Arrokoth, and more importantly, that Arrokoth's present spin period may indeed reflect a rather low bulk density near  $250 \text{ kg m}^{-3}$ , a density for which there is independent geophysical evidence (Keane et al., 2020; McKinnon et al., 2020).

The case of comet 103P/Hartley 2, visited by the *EPOXI* spacecraft in 2010 (A'Hearn et al., 2011), is of some interest in this regard. This comet possesses a bilobate structure and a very low rotation rate (18.3 hr), similar to that of Arrokoth, though much smaller in size. It has a very smooth neck region, which when interpreted as an equipotential surface, implies a bulk density of 220 (140–520)  $\text{kg m}^{-3}$  (Richardson & Bowling, 2014).

The most massive impactors have the greatest effect on spin evolution, so we directed special attention to the crater Sky (formerly Maryland), which is located closer to the leading side (with respect to the body's rotation) of Arrokoth's Small Lobe. This single impact dominates all others known in terms of Arrokoth's spin evolution, and is reasonably well positioned to reduce Arrokoth's spin (though, from the geometry in Figure 8, may spin Arrokoth up as well). We recognize that the largest crater or craters on the unilluminated, non-encounter side of Arrokoth remain unknown, but Sky serves as a proxy to study the effects of the largest impacts, and in greater detail.

We use a Monte Carlo approach to examine all likely combinations of impactor size, speed and angle that might have created Sky at its actual position, and determined the range of angular momentum changes for Arrokoth's true three-dimensional bilobate shape. We find an essentially similar range of spin changes, either up or down, as in our initial suites of calculations, as a function of Arrokoth's assumed bulk density (remembering that we vary impactor and target density simultaneously, based on the idea that the mean density of all small classical Kuiper belt objects, whatever it may be, is likely similar).

We also tested specifically whether suppressing ejecta (a hallmark of compaction cratering (Housen et al., 2018)) makes a significant difference in momentum transfer and spin evolution. It does not, because in the gravity regime most ejecta, even ejecta that escapes, moves at much lower speeds than the impactor's collision speed. For example, for a typical Sky-forming cold classical impactor (1-km diameter,  $300 \text{ m s}^{-1}$ , impacting at  $45^\circ$ ), the momentum carried away in the escaping ejecta is about 30% of the incoming impactor, giving a total momentum transfer  $\beta$  of 1.3. This is not an atypical  $\beta$  value for a strengthless, granular target (Holsapple & Housen, 2012).

The densities we examine for Arrokoth range from that of comet 67P/Churyumov-Gerasimenko (well-determined) down to the minimum suggested from Arrokoth's spin period and distribution of surface slopes (McKinnon et al., 2020; Spencer et al., 2020). This range (250-to- $500 \text{ kg m}^{-3}$ ) implies a considerable porosity when compared with a nominal grain density of KBO-forming material of perhaps  $1,800 \text{ kg m}^{-3}$  (e.g., Bierson et al., 2018; McKinnon et al., 2017). Accordingly we also implement the highly porous crater scaling proposed by Housen et al. (2018) for Arrokoth, in the gravity regime. This scaling provides an excellent match, for example, for experimental craters formed in highly porous, granular pumice (Housen et al., 2018), data that show a marked reduction in crating efficiency with respect to dry sand or cohesionless regolith. Accordingly, Sky-forming impactors need to be larger, and we find that impact spindown of Arrokoth cannot be statistically rejected for bulk densities  $\lesssim 400 \text{ kg m}^{-3}$  (initial synchronous spin periods  $\gtrsim 12.5 \text{ hr}$ ). But this is not the same as saying spindown is likely. We conclude that based on these porous-scaling results Arrokoth's spin state may not actually be truly primordial, but could have been spinning up to some 25% faster when its two lobes first merged. Together, all of the results we present support the geophysical inference that Arrokoth is most likely a truly remarkably low-density body. Such a low density (most likely near  $300 \text{ kg m}^{-3}$ ) would be a surviving signature of Arrokoth's accretion, its cold classical primordial structure and composition fundamentally unmodified by later collisional or thermal evolution.

## Data Availability Statement

All data used in the manuscript are publicly accessible from Figshare data repository (Mao, 2021).

## Acknowledgments

This work supported by NASA New Horizons project (contracts NASW-02008 and NAS5-97271/TaskOrder30), and made possible by New Horizon's successful flyby of Arrokoth and its continuing operation. A portion of this work was carried out at the Jet Propulsion Laboratory, California Institute of Technology, under a contract with the National Aeronautics and Space Administration (80NM0018D0004). We thank James Richardson and an anonymous reviewer for their comments.

## References

- Abedin, A. Y., Kavelaars, J. J., Greenstreet, S., Petit, J.-M., Gladman, B., Lawler, S., et al. (2021). OSSOS. XXI. Collision probabilities in the Edgeworth–Kuiper Belt. *The Astronomical Journal*, *161*(4), 195. <https://doi.org/10.3847/1538-3881/abe418>
- A'Hearn, M. F., Belton, M. J. S., Delamere, W. A., Feaga, L. M., Hampton, D., Kissel, J., et al. (2011). EPOXI at comet Hartley 2. *Science*, *332*(6036), 1396–1400. <https://doi.org/10.1126/science.1204054>
- Bierson, C. J., & Nimmo, F. (2019). Using the density of Kuiper belt objects to constrain their composition and formation history. *Icarus*, *326*, 10–17. <https://doi.org/10.1016/j.icarus.2019.01.027>
- Bierson, C. J., Nimmo, F., & McKinnon, W. B. (2018). Implications of the observed Pluto–Charon density contrast. *Icarus*, *309*, 207–219. <https://doi.org/10.1016/j.icarus.2018.03.007>
- Buie, M. W., Porter, S. B., Tamblin, P., Terrell, D., Parker, A. H., Baratoux, D., et al. (2020). Size and shape constraints of (486958) Arrokoth from stellar occultations. *The Astronomical Journal*, *159*, 130. <https://doi.org/10.3847/1538-3881/ab6ced>
- Burns, J. A., Safronov, V. S., & Gold, T. (1973). Asteroid nutation angles. *Monthly Notices of the Royal Astronomical Society*, *165*, 403–411. <https://doi.org/10.1093/mnras/165.4.403>
- Cheng, A. F., Stickle, A. M., Fahnestock, E. G., Dotto, E., Della Corte, V., Chabot, N. L., & Rivkin, A. S. (2020). DART mission determination of momentum transfer: Model of ejecta plume observations. *Icarus*, *352*, 113989. <https://doi.org/10.1016/j.icarus.2020.113989>
- Dobrovolskis, A. R., & Burns, J. A. (1980). Life near the Roche limit: Behavior of ejecta from satellites close to planets. *Icarus*, *42*(3), 422–441. [https://doi.org/10.1016/0019-1035\(80\)90105-0](https://doi.org/10.1016/0019-1035(80)90105-0)

- Dobrovolskis, A. R., & Burns, J. A. (1984). Angular momentum drain: A mechanism for despinning asteroids. *Icarus*, 57(3), 464–476. [https://doi.org/10.1016/0019-1035\(84\)90130-1](https://doi.org/10.1016/0019-1035(84)90130-1)
- Fu, R. R., Hager, B. H., Ermakov, A. I., & Zuber, M. T. (2014). Efficient early global relaxation of asteroid Vesta. *Icarus*, 240, 133–145. <https://doi.org/10.1016/j.icarus.2014.01.023>
- Goldreich, P., & Sari, R. (2009). Tidal evolution of rubble piles. *The Astrophysical Journal*, 691(1), 54–60. <https://doi.org/10.1088/0004-637X/691/1/54>
- Goldreich, P., & Soter, S. (1966). Q in the solar system. *Icarus*, 5(1), 375–389. [https://doi.org/10.1016/0019-1035\(66\)90051-0](https://doi.org/10.1016/0019-1035(66)90051-0)
- Greenstreet, S., Gladman, B., McKinnon, W. B., Kavelaars, J. J., & Singer, K. N. (2019). Crater density predictions for New Horizons flyby target 2014 MU69. *The Astrophysical Journal Letters*, 872(1), L5. <https://doi.org/10.3847/2041-8213/ab01db>
- Grishin, E., Malamud, U., Perets, H. B., Wandel, O., & Schäfer, C. M. (2020). The wide-binary origin of (2014) MU69-like Kuiper belt contact binaries. *Nature*, 580(7804), 463–466. <https://doi.org/10.1038/s41586-020-2194-z>
- Groussin, O., Attree, N., Broutet, Y., Ciarletti, V., Davidsson, B., Filacchione, G., et al. (2019). The thermal, mechanical, structural, and dielectric properties of cometary nuclei after Rosetta. *Space Science Reviews*, 215(4), 29. <https://doi.org/10.1007/s11214-019-0594-x>
- Grundy, W. M., Bird, M. K., Britt, D. T., Cook, J. C., Cruikshank, D. P., Howett, C. J. A., et al. (2020). Color, composition, and thermal environment of Kuiper Belt object (486958) Arrokoth. *Science*, 367(6481), eaay3705. <https://doi.org/10.1126/science.aay3705>
- Henych, T., & Pravec, P. (2013). Asteroid rotation excitation by subcatastrophic impacts. *Monthly Notices of the Royal Astronomical Society*, 432(2), 1623–1631. <https://doi.org/10.1093/mnras/stt581>
- Hirabayashi, M., Trowbridge, A. J., & Bodewits, D. (2020). The mysterious location of Maryland on 2014 MU69 and the reconfiguration of its bilobate shape. *The Astrophysical Journal Letters*, 891(1), L12. <https://doi.org/10.3847/2041-8213/ab3e74>
- Holsapple, K. A. (1993). The scaling of impact processes in planetary sciences. *Annual Review of Earth and Planetary Sciences*, 21, 333–373. <https://doi.org/10.1146/annurev.ea.21.050193.002001>
- Holsapple, K. A., & Housen, K. R. (2012). Momentum transfer in asteroid impacts. I. Theory and scaling. *Icarus*, 221(2), 875–887. <https://doi.org/10.1016/j.icarus.2012.09.022>
- Holsapple, K. A., & Housen, K. R. (2019). The catastrophic disruptions of asteroids: History, features, new constraints and interpretations. *Planetary and Space Science*, 179, 104724. <https://doi.org/10.1016/j.pss.2019.104724>
- Housen, K. R., & Holsapple, K. A. (2011). Ejecta from impact craters. *Icarus*, 211(1), 856–875. <https://doi.org/10.1016/j.icarus.2010.09.017>
- Housen, K. R., Sweet, W. J., & Holsapple, K. A. (2018). Impacts into porous asteroids. *Icarus*, 300, 72–96. <https://doi.org/10.1016/j.icarus.2017.08.019>
- Keane, J. T., Porter, S. B., Beyer, R. A., Umurhan, O. M., McKinnon, W. B., Moore, J. M., et al. (2020). Geophysics of (486958) Arrokoth revealed by New Horizons. In *AAS/Division of Planetary Science Meeting #52*, id. 508.02.
- Lisse, C. M., Young, L. A., Cruikshank, D. P., Sandford, S. A., Schmitt, B., Stern, S. A., et al. (2021). On the origin & thermal stability of Arrokoth's and Pluto's ices. *Icarus*, 356, 114072. <https://doi.org/10.1016/j.icarus.2020.114072>
- Lyra, W., Youdin, A. N., & Johansen, A. (2021). Evolution of MU69 from a binary planetesimal into contact by Kozai-Lidov oscillations and nebular drag. *Icarus*, 356, 113831. <https://doi.org/10.1016/j.icarus.2020.113831>
- MacMillan, W. D. (1930). *The theory of the potential*. McGraw-Hill.
- Mao, X. (2021). Simulation data for manuscript "Collisions by small Kuiper belt objects with (486958) Arrokoth: Implications for its spin evolution and bulk density" [Data set]. Figshare. <https://doi.org/10.6084/m9.figshare.14573637..>
- Mao, X., & McKinnon, W. B. (2020). Spin evolution of Ceres and Vesta due to impacts. *Meteoritics & Planetary Sciences*, 55(11), 2493–2518. <https://doi.org/10.1111/maps.13594>
- Mao, X., McKinnon, W. B., Singer, K. N., Keane, J. T., Robbins, S. J., Schenk, P. M., et al. (2020a). Investigating possible spindown of Arrokoth by collisions with small classical Kuiper belt objects. In *Europlanet Science Congress*, abs# EPSC2020-553.
- Mao, X., McKinnon, W. B., Singer, K. N., Keane, J. T., Robbins, S. J., Schenk, P. M., et al. (2020b). Merger and spindown of (486958) Arrokoth by collisions. In *51st Lunar and Planetary Science Conference*. abs. #2592.
- McKinnon, W. B., Mao, X., Singer, K. N., Keane, J. T., Schenk, P. M., White, O. L., et al. (2021). Are Maryland and other craters on CCKBO Arrokoth compaction craters, and does it matter? In *52nd Lunar and Planetary Science Conference*, abs #2719.
- McKinnon, W. B., Richardson, D. C., Marohnic, J. C., Keane, J. T., Grundy, W. M., Hamilton, D. P., et al. (2020). The solar nebula origin of (486958) Arrokoth, a primordial contact binary in the Kuiper Belt. *Science*, 367(6481), eaay6620. <https://doi.org/10.1126/science.aay6620>
- McKinnon, W. B., Stern, S. A., Weaver, H. A., Nimmo, F., Bierson, C. J., Grundy, W. M., et al. (2017). Origin of the Pluto–Charon system: Constraints from the New Horizons flyby. *Icarus*, 287, 2–11. <https://doi.org/10.1016/j.icarus.2016.11.019>
- McKinnon, W. B., Stern, S. A., Weaver, H. A., Spencer, J. R., Buie, M. W., Beyer, R. A., et al. (2019). A pristine "contact binary" in the Kuiper Belt: Implications from the New Horizons encounter with 2014 MU69 ("Ultima Thule"). In *50th Lunar and Planetary Science Conference*, abs. #2767.
- Morbidelli, A., & Nesvorný, D. (2020). Kuiper belt: Formation and evolution. In D. Prialnik, M. A. Barucci, & L. Young (Eds.), *The Trans-Neptunian solar system* (pp. 25–59). Elsevier. <https://doi.org/10.1016/B978-0-12-816490-7.00002-3>
- Morbidelli, A., Nesvorný, D., Bottke, W. F., & Marchi, S. (2021). A re-assessment of the Kuiper belt size distribution for sub-kilometer objects, revealing collisional equilibrium at small sizes. *Icarus*, 356, 114256. <https://doi.org/10.1016/j.icarus.2020.114256>
- Nesvorný, D., Li, R., Simon, J. B., Youdin, A. N., Richardson, D. C., Marschall, R., & Grundy, W. M. (2021). Binary planetesimal formation from gravitationally collapsing pebble clouds. *The Planetary Science Journal*, 2(1), 27. <https://doi.org/10.3847/psj/abd858>
- Nesvorný, D., Li, R., Youdin, A. N., Simon, J. B., & Grundy, W. M. (2019). Trans-Neptunian binaries as evidence for planetesimal formation by the streaming instability. *Nature Astronomy*, 3(9), 808–812. <https://doi.org/10.1038/s41550-019-0806-z>
- Nesvorný, D., Youdin, A. N., & Richardson, D. C. (2010). Formation of Kuiper Belt binaries by gravitational collapse. *The Astronomical Journal*, 140(3), 785–793. <https://doi.org/10.1088/0004-6256/140/3/785>
- Petrenko, V. F., & Whitworth, R. W. (2002). *Physics of ice*. Oxford University Press. <https://doi.org/10.1093/acprof:oso/9780198518945.001.0001>
- Richardson, J. E. (2011). Modeling impact ejecta plume evolution: A comparison to laboratory studies. *Journal of Geophysical Research E: Planets*, 116(12), E12004. <https://doi.org/10.1029/2011JE003844>
- Richardson, J. E., & Bowling, T. J. (2014). Investigating the combined effects of shape, density, and rotation on small body surface slopes and erosion rates. *Icarus*, 234, 53–65. <https://doi.org/10.1016/j.icarus.2014.02.015>
- Schenk, P., Singer, K., Beyer, R., Beddingfield, C., Robbins, S. J., McKinnon, W. B., et al. (2021). Origins of pits and troughs and degradation on a small primitive planetesimal in the Kuiper Belt: High-resolution topography of (486958) Arrokoth (aka 2014 MU69) from New Horizons. *Icarus*, 356, 113834. <https://doi.org/10.1016/j.icarus.2020.113834>
- Singer, K. N., McKinnon, W. B., Gladman, B., Greenstreet, S., Bierhaus, E. B., Stern, S. A., et al. (2019a). Impact craters on Pluto and Charon indicate a deficit of small Kuiper belt objects. *Science*, 363(6430), 955–959. <https://doi.org/10.1126/science.aap8628>

- Singer, K. N., McKinnon, W. B., & Nowicki, L. T. (2013). Secondary craters from large impacts on Europa and Ganymede: Ejecta size-velocity distributions on icy worlds, and the scaling of ejected blocks. *Icarus*, 226(1), 865–884. <https://doi.org/10.1016/j.icarus.2013.06.034>
- Singer, K. N., Spencer, J. R., McKinnon, W. B., Stern, S. A., Greenstreet, S., Gladman, B., et al. (2019b). Impact craters on 2014 MU69: Implications for Kuiper belt object size-frequency distributions and planetesimal formation. In *AGU Fall Meeting, abs. #P331-3535*.
- Spencer, J. R., Stern, S. A., Moore, J. M., Weaver, H. A., Singer, K. N., Olkin, C. B., et al. (2020). The geology and geophysics of Kuiper Belt object (486958) Arrokoth. *Science*, 367(6481), aay3999. <https://doi.org/10.1126/science.aay3999>
- Stern, S. A., Keeney, B., Singer, K. N., White, O., Hofgartner, J. D., & Grundy, W. (2021). Some new results and perspectives regarding the Kuiper Belt object Arrokoth's remarkable, bright neck. *The Planetary Science Journal*, 2(3), 87. <https://doi.org/10.3847/psj/abee26>
- Stern, S. A., Weaver, H. A., Spencer, J. R., Olkin, C. B., Gladstone, G. R., Grundy, W. M., et al. (2019). Initial results from the New Horizons exploration of 2014 MU69, a small Kuiper Belt object. *Science*, 364(6441), eaaw9771. <https://doi.org/10.1126/science.aaw9771>

## References From the Supporting Information

- Chen, T., & Glotzer, S. C. (2007). Simulation studies of a phenomenological model for elongated virus capsid formation. *Physical Review E*, 75(5), 051504. <https://doi.org/10.1103/PhysRevE.75.051504>
- Williamson, J. F. (1987). Random selection of points distributed on curved surfaces. *Physics in Medicine and Biology*, 32(10), 1311–1319. <https://doi.org/10.1088/0031-9155/32/10/009>